The Design and Applications of Highly Dispersive Acoustic Surface-Wave Filters

HENRY M. GERARD, W. RICHARD SMITH, WILLIAM R. JONES, AND J. BENJAMIN HARRINGTON

Invited Paper

Abstract—**The development of a low-loss broad-band linear FM dispersive filter having a time–bandwidth (TB) product of 1000 is discussed. Two systems applications for highly dispersive linear FM filters—pulse compression radar and a microscan receiver—are discussed with emphasis on filter performance requirements. The principal factors which influence the design of surface-wave filters are reviewed and theoretical design procedures are outlined. The 1000:1 filters, which are implemented on strong-coupling *YZ* lithium niobate, typically meet the design goal of a 100-MHz rectangular passband and have a CW insertion loss of less than 35 dB. Measured data are presented for the filter performance in a pulse-compression loop and in a prototype broad-band microscan (compressive) receiver.**

I. Introduction

THEIR SIZE, design flexibility, and reproducibility make acoustic surface-wave devices excellent candidates for many important applications in radar and communication systems. This paper discusses applications, design, and fabrication of highly dispersive filters (HDF's) as a specific class of surface-wave devices.

A dispersive filter is a delay line whose group delay is a nonconstant function of the instantaneous frequency of the input signal, and whose amplitude response is generally shaped for its specific application. In particular, a linear FM dispersive filter is designed to have a linear group delay versus frequency. Because of their importance, we will concentrate our attention on linear FM dispersive filters; however, the basic concepts apply equally well to the broader class.

For the purpose of this paper, we arbitrarily define a *highly dispersive* filter as one with a time–bandwidth (TB) product of $\Delta\tau\Delta f \gtrsim 1000$, where $\Delta\tau$ is the differential time delay and Δf is the filter bandwidth.

Although there are many applications for dispersive filters, the discussion in Section II is confined to pulse-compression radar and the microscan, or compressive, receiver. This section emphasizes the importance of highly dispersive pulse-compression filters for meeting the present-day requirements of these systems. Section III continues with an overview of the design considerations for a highly dispersive filter. Such factors as insertion loss, bandwidth, and time dispersion are herein related to the transducer geometry and choice of substrate. This is followed by a review of the design theory, which demonstrates the extent to which current transducer circuit models may be employed in the design and analysis of complex dispersive filters.

Manuscript received September 15, 1972; revised October 16, 1972. This work was supported in part by the U.S. Army Electronics Command, Fort Monmouth, N. J., under Contract DAAB-07-71-C-0046, and in part by the Rome Air Development Center, Griffiss Air Force Base, Rome, N. Y., under Contract F30602-71-C-0347.

The authors are with the Hughes Aircraft Company, Ground Systems Group, Fullerton, Calif. 92634.

In Section V the performance of a low-loss 100-MHz bandwidth 1000:1 linear FM dispersive filter is presented with filter errors treated in detail.

In the final section, some new techniques are discussed which promise to extend the realm of acoustic surface-wave filter capabilities to meet future requirements.

II. Applications

Pulse-Compression Radar

HDF's are of special interest for application to large TB pulse-compression radars. The purpose of using large TB dispersive filters is to implement long-range high-range resolution radar systems for the detection, identification, and tracking of high-speed airborne objects.

The linear FM dispersive filter is by far the most extensively studied and widely used in radar applications [1]. This may be traced to the simplicity of linear FM filter design and the inherent tolerance of the linear FM waveform to Doppler-shifted returns from high-velocity targets.

A pulse-compression radar system may generate the frequency-modulated pulse by applying a short pulse to the input of a dispersive filter. The "chirped" output pulse is spread in time and peak-power reduced by a factor equal to the TB product of the filter. This stretched pulse is frequency-converted to the radar RF, amplified, and transmitted. The received target returns are amplified, down-converted to the receiver IF, and compressed in a matched dispersive filter. This compression increases the peak amplitude of the returning signals and reduces their time duration by the TB product, i.e., the compression ratio. Spreading the signal in time upon transmission increases the radar range by permitting the peak power-limited transmitter to radiate more energy per pulse. However, the signal sensitivity and dynamic range thus gained are decreased by the insertion loss incurred during pulse expansion. Thus the dispersive-filter insertion loss is a critical factor in determining the maximum dynamic range of a chirp radar system.

Detecting, identifying, and tracking high-speed airborne objects require range resolution of 1–2 m and velocity resolution on the order of 1000 m/s. Range resolution ΔR and Doppler velocity resolution ΔV are related to signal bandwidth Δf and pulse duration $\Delta\tau$ as

$$\Delta R \simeq \frac{c}{2\Delta f} \tag{2-1}$$

and

$$\Delta V \simeq \frac{c}{2f_0\Delta\tau} \tag{2-2}$$

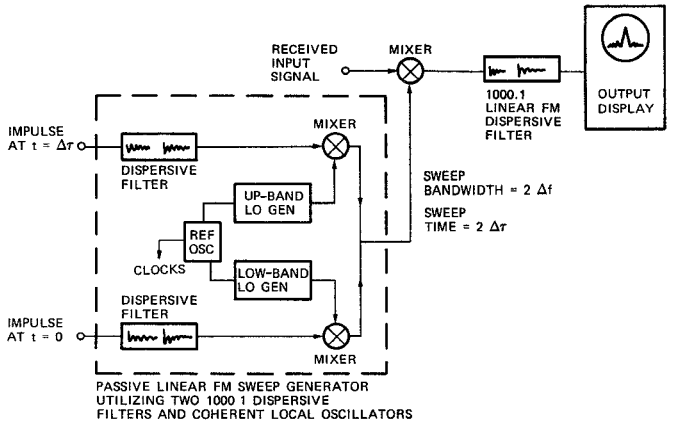

Fig. 1. Block diagram of microscan or compressive receiver, utilizing large TB product linear FM dispersive filters and passively generated sweep.

where f_0 is the radar carrier frequency and c is the speed of light.[1] For a typical 3-GHz radar, the above resolutions require $\Delta f \simeq 100$ MHz and $\Delta\tau \simeq 50$ μs. From this example, it is clear that TB products ($\Delta f \Delta\tau$) of several thousand are needed. Consequently, we have chosen to define a highly dispersive filter as one having a TB product in excess of 1000.

Microscan (Compressive) Receiver

The microscan receiver, sometimes referred to as a compressive receiver, is used to detect and instantaneously measure the frequencies of unknown signals. This type of receiver is essentially a fast spectrum analyzer equivalent to a contiguous filter bank of up to several thousand filters.

The basic design, Fig. 1, differs from a conventional receiver in that the center frequency is controlled by a sweeping local oscillator (dashed box in Fig. 1). The LO sweep, which may be generated by a linear FM dispersive filter, produces a signal whose frequency sweeps linearly over a band B in time T. In the specific implementation, two 1000:1 dispersive filters are combined (with appropriate frequency translation) to generate a sweep having $B = 2\Delta f$ and $T = 2\Delta\tau$. Since the dispersive filter following the mixer acts as a matched filter by compressing the signal that was modulated by the sweeping LO, the frequency versus time slope of this compression filter must match the sweep rate of the local oscillator.

The receiver operation may be clarified using the sweep-intercept diagram shown in Fig. 2, in which the mixer output frequency is plotted as a function of time. A typical displayed output, as shown at the bottom of Fig. 2, contains one compressed pulse for each received frequency. The time delay of the compressed output pulse is determined by the specific portion of the LO sweep that is mixed down to the compression filter band. Thus the frequency of the received signal, which controls the frequency translation of the sweep, also controls the time of the output pulse. That is, two signals differing in frequency by δf produce displayed pulses that are separated in time by $\delta t = (\Delta\tau/\Delta f)\delta f$.

The two intercepted CW signals superimposed on the response diagram represent the highest and lowest frequencies ($f_{s\max}$ and $f_{s\min}$) that can be resolved using the full bandwidth of the compression filter. The criterion for full resolution is that the mixer output signal for the received frequency com-

[1] For a more general treatment of range and velocity resolution see [16].

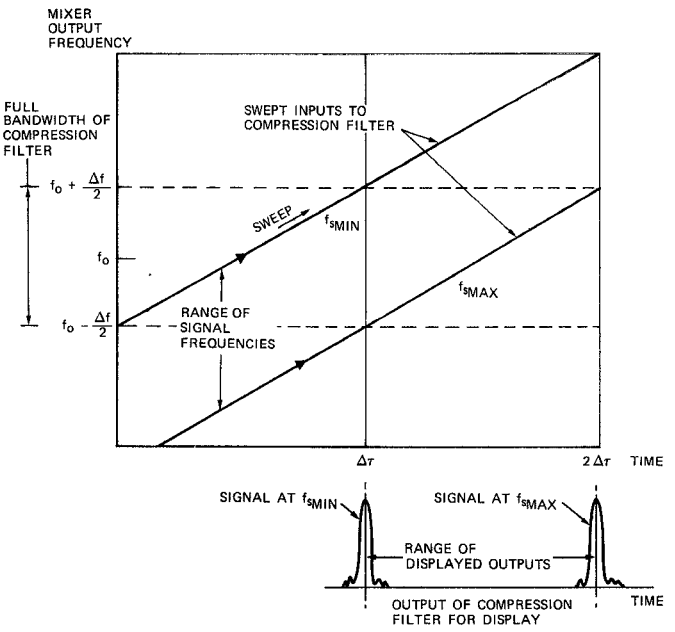

Fig. 2. Sweep diagram for sweep range, $B = 2\Delta f$, and sweep time, $T = 2\Delta\tau$, showing compressed outputs for two input frequencies.

pletely span the frequency range $|f - f_0| \leq \Delta f/2$, which defines the passband of the compression filter. If the mixer output signal does not cover the full band of the compression filter, the effective compression ratio is reduced, and the output corresponding to that frequency will not have the full-time (hence frequency) resolution.

The range of signal frequencies f_s over which full resolution occurs is shown in Fig. 2 for the particular receiver described above, in which the local oscillator frequency (f_{LO}) sweeps over the range $|f_{LO} - f_0| = \Delta f$. In general, it can be shown that the range of full-frequency resolution is equal to the sweep range minus the compression-filter bandwidth.

After compression, the time resolution is

$$\Delta t \simeq \frac{1}{\Delta f} \tag{2-3}$$

which gives a frequency resolution of

$$\delta f_r \simeq \Delta t\left(\frac{\Delta f}{\Delta\tau}\right) = \frac{1}{\Delta\tau}. \tag{2-4}$$

To achieve high-frequency resolution, large dispersion is required in the compression filters. Moreover, high sweep rates $\Delta f/\Delta\tau$ are required to cover large bandwidths in minimum time. Since the compression filter requires a large TB product, highly dispersive filters are an attractive candidate for this application.

III. Overview of Design Considerations

The dispersive filter design requires determining a surface-wave filter with an impulse response specified in the time domain as

$$h(t) = e(t) \exp\left[j\phi(t)\right] \tag{3-1}$$

or in the frequency domain as

$$H(f) = E(f) \exp\left[j\Phi(f)\right]. \tag{3-2}$$

This paper concentrates on a linear FM waveform of center frequency f_0, pulse length $\Delta\tau$, chirp bandwidth Δf, and an im-

pulse response

$$h(t) = \begin{cases} \exp\left[j2\pi\left(f_0 t + \dfrac{\Delta f}{\Delta\tau}\dfrac{t^2}{2}\right)\right], & |t| < \dfrac{\Delta\tau}{2} \\ 0, & |t| > \dfrac{\Delta\tau}{2}. \end{cases} \quad (3\text{-}3)$$

The surface-wave filter is treated as a two-port network whose terminal pairs are the electrical terminals of the two surface-wave transducers. The voltage transfer function $T(f)$ of this network, when loaded, is required to be

$$T(f) = A \exp\left[-j2\pi f\tau\right]H(f) \quad (3\text{-}4)$$

i.e., $T(f)$ must be made equal to the desired spectrum to within a nondispersive delay τ and a constant A. The constant A is maximized when the transducer and external circuit are matched for minimum insertion loss.

Important limitations which influence the construction of a highly dispersive surface-wave filter satisfying (3-4) are enumerated below.

1) The pulse length $\Delta\tau$ of a single filter is limited by the length of the piezoelectric crystal. The length is also limited by the increase in acoustic propagation loss proportional to the number of electrodes ($N \simeq 2f_0\Delta\tau$).

2) The center frequency (f_0) is limited to about 300 MHz by the state of the art in photolithography.

3) The fractional bandwidth ($\Delta f/f_0$) limitation depends on whether the filter is configured with one dispersive transducer and one nondispersive transducer or with two dispersive transducers. Ordinary periodic nondispersive transducer fractional bandwidths are limited to about 0.25, with new types of nondispersive transducers showing promise for fractional bandwidths up to 0.4. Using a pair of dispersive transducers divides the total pulse length between two transducers, requiring that their *combined* response satisfy (3-4). The fractional bandwidth of dispersive transducers is limited to less than 1.0 to prevent the low-frequency electrodes, synchronous at $f_0-(\Delta f/2)$, from generating interfering third harmonic signals at $f_0+(\Delta f/2)$. If no special bulk wave suppression techniques are employed, the fractional bandwidth should be somewhat smaller than 1.0 to prevent the low-frequency electrodes from generating bulk waves when operated at $f_0+(\Delta f/2)$.

4) The apodization (acoustic aperture tapering) required to produce the desired amplitude response $E(f)$ can complicate the design theory. When both transducers are apodized, the circuit model [2] may fail, since it does not model the complicated double sum required to account for the response of each electrode in the receiving transducer to the acoustic waves from each electrode in the launching transducer [3]. Designs with only one apodized transducer circumvent this problem.

5) The low ($<50\ \Omega$) transducer impedance requires the use of low-loss broad-band matching networks. The transducer impedance is low because large numbers of electrodes lead to a large capacitance and radiation conductance, which cannot be reduced by use of a narrow aperture because of diffraction limitations.

6) A compression filter with temporal amplitude weighting for compressed-pulse sidelobe suppression is subject to acoustic diffraction problems. This is because highly tapered transducer apertures are needed to implement amplitude weighting directly into the acoustic filter via the function $e(t)$ in (3-1). An external weighting filter eliminates this problem.

7) Large acoustic multiple-transit echoes can occur in highly dispersive filters implemented on strong-coupling piezoelectric materials (such as *YZ* lithium niobate) which are attractive for low insertion-loss applications. The strong coupling causes a relatively large perturbation in the acoustic-wave impedance under the metal electrodes. The resultant small acoustic reflections from each electrode can add in phase to give large multiple-transit echoes [2]. The "double electrode" technique [4] eliminates this problem, but the required fabrication process becomes intractable at high frequencies. Fortunately, the problem is ameliorated in large TB filters inasmuch as the multiple-transit echoes undergo a large decorrelation suppression relative to the desired signal and are also attenuated by propagation loss.

IV. Filter Design and Analysis

In order to implement a surface-wave filter it is necessary to choose a scheme for employing *two* transducers which together produce the desired frequency response. Specifically, it is necessary to find two new signals from which the two individual transducers are to be designed. One method is to use a short unapodized nondispersive transducer[2] whose spectral amplitude response is nearly constant over the desired bandwidth Δf. Such a transducer launches a straight-crested wave whose transverse energy distribution is uniform (ignoring diffraction effects in the near field). In this case the filter transfer function $T(f)$ assumes the product form

$$T(f) = T_1(f)\cdot T_2(f) \quad (4\text{-}1)$$

where $T_1(f)$, the electroacoustic transfer function of the nondispersive transducer, is approximately

$$T_1(f) \cong A_1 \exp\left[-j2\pi f\tau_1\right] \quad (4\text{-}2)$$

and $T_2(f)$, associated with the dispersive transducer, is to be designed from the relation

$$T_2(f) = (A/A_1)\exp\left[-j2\pi f(\tau - \tau_1)\right]H(f). \quad (4\text{-}3)$$

Thus one transducer has a transfer function of the same form (3-4) as specified for the entire filter. The main disadvantage of this configuration is the inherent bandwidth limitation of the nondispersive transducer. Broad bandwidth operation can be achieved by dividing the differential time delay $\Delta\tau$ between two identical apodized transducers each having bandwidth Δf. Reference [3] shows that the transfer function of a filter employing two apodized transducers, in general, cannot be described by the product of the individual transducer transfer functions. However, the product form (4-1) is a good approximation if the apodized transducers are identical and the compression ratio is very large.

The desired impulse response can be synthesized by using two identical apodized transducers whose common electroacoustic transfer function is $\sqrt{H(f)}$, where $H(f)$ is given by (3-2). The desired filter impulse response is the linear FM waveform given by (3-3). If we denote the Fourier transform by F, the resulting time signal for each transducer is $h_1(t) = F^{-1}\{\sqrt{F[h(t)]}\}$. For large $\Delta\tau\Delta f$, $h_1(t)$ is approximately a

[2] A periodic transducer or any transducer with a plane of symmetry normal to the propagation direction is nondispersive.

linear FM waveform given by

$$h_1(t) \cong \begin{cases} \exp\left[j2\pi\left(f_0 t + \frac{\Delta f}{\Delta \tau} t^2\right)\right], & |t| < \frac{\Delta \tau}{4} \\ 0, & |t| > \frac{\Delta \tau}{4}. \end{cases} \quad (4\text{-}4)$$

The filter-synthesis problem is thus reduced to designing a transducer which produces the impulse response $h_1(t)$ given by (4-4).

According to the naive linear FM prescription, the transducer electrodes should be placed at temporal positions given by

$$2\left(f_0 t_n + \frac{\Delta f}{\Delta \tau} t_n^2\right) = \left(n - \frac{N_1}{2}\right) \quad (4\text{-}5)$$

where $N_1 = f_0 \Delta \tau + 1$ is the number of electrodes in each transducer. Reference [2] shows that (4-5) must be modified because of the interaction between the acoustic waves and electric load. The modified equation is

$$2\left(f_0 t_n + \frac{\Delta f}{\Delta \tau} t_n^2\right) + \tan^{-1}\left\{\frac{Q_L}{f_0}\left(f_0 + \frac{2\Delta f}{\Delta \tau} t_n\right)\right\} = \left(n - \frac{N_1}{2}\right). \quad (4\text{-}6)$$

The parameter measuring the interaction is the "load Q," defined by

$$Q_L = 2\pi f_0 C_T R_L \quad (4\text{-}7)$$

where R_L is the load resistance and C_T is the transducer capacitance.

There are at least two additional effects which require further modification of the electrode-positioning law (4-6). One is the difference in the surface-wave velocity in the metallized electrode regions compared to that in the gaps between electrodes. If the transducer is constructed with the electrode width being a constant fraction of the spacing between adjacent line centers, (4-6) remains valid provided that an "effective" surface-wave velocity [5] is used in converting from temporal electrode positions to spatial positions ($x_n = v_{\text{eff}} t_n$). However, common techniques for fabrication of high-frequency transducer patterns generally dictate a constant electrode width. The required modification to the spatial electrode positions is described in [5] for the case corresponding to $Q_L = 0$. Another effect is velocity dispersion due to finite-thickness electrodes. This problem becomes increasingly serious as the design frequency of the filter is increased.

Completion of the transducer design consists of specifying the acoustic apertures (w_n) of the electrodes; that is, the length of overlap of adjacent electrodes measured in the direction transverse to acoustic propagation. For linear FM transducers of large compression ratio, the apertures are given to an excellent approximation by [2]

$$w_n \propto \left(\frac{f_n}{f_0}\right)^{-3}\left[1 + Q_L\left(\frac{f_n}{f_0}\right)^2\right] \quad (4\text{-}8)$$

where f_n is the synchronous frequency defined by $f_n = (t_{n+1} - t_n)^{-1}$. Note that the apertures are wider at the low-frequency end than at the high-frequency end of the transducer, and for weak coupling to the load ($Q_L \to 0$), the apertures vary as f_n^{-3}. Slight modifications to (4-8) are required to compensate for electrostatic electric field variations if all transducer electrodes have the same width.[3]

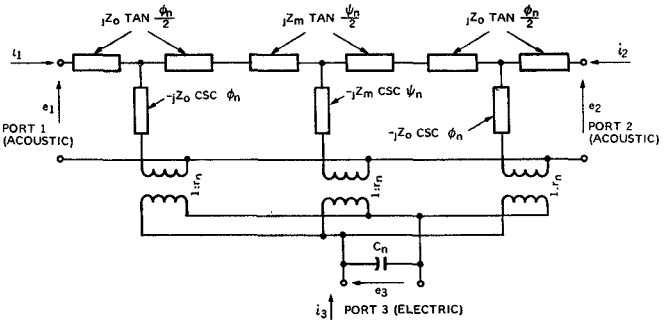

Fig. 3. Mason equivalent circuit for the crossed-field model of one electrode including an acoustic impedance discontinuity.

The 1000:1 linear FM transducer design incorporated the modifications outlined above and was implemented using an iterative numerical procedure to derive the electrode pattern.

Detailed calculations of filter performance are carried out by use of the crossed-field Mason circuit model [6], modified to include acoustic-propagation loss, velocity dispersion under the metal electrodes, and different acoustic-wave impedances in the electrode and gap regions. The three-port circuit for one electrode plus half of each adjacent gap is shown in Fig. 3. The metallized region has an acoustic impedance Z_m and transit angle $\psi_n = 2\pi f L_{sn}/v_m$, where L_{sn} is the width of the nth electrode and v_m is the acoustic velocity in the metallized region. In general, v_m is taken to be a frequency-dependent function of the form v_1—khf, where k is a constant of the materials, h is the electrode thickness, and f is the operating frequency. The gap region consisting of half of each gap adjacent to the nth electrode has length L_{gn}, and is represented by two transmission lines, each of impedance Z_0 and transit angle $\phi_n = \pi f L_{gn}/v_0$, where v_0 is the surface-wave velocity of the unmetallized region. Evaluation of the effect of acoustic-propagation loss requires the inclusion of imaginary parts of Z_0, Z_m, ϕ_n, and ψ_n. Reference [2] gives further details of the electrode capacitance C_n, electroacoustic transformers, and interconnection of the single-electrode networks into a transducer circuit.

The computer program which utilizes the above model for transducer analysis also combines transducers to find the frequency-domain response of a dispersive filter. In addition, it finds the response of a pulse-compression loop (expansion and compression filters with optional spectral weighting filter), giving frequency-domain amplitude and phase information as well as compressed pulses in the time domain.

The analytical model confirms the effectiveness of designing the transducers to account for a reduced, dispersive velocity under metal electrodes and for coupling to the electric load. When these effects are not taken into account in the transducer design, the result is phase errors which in turn cause severe distortion of the recompressed pulse and associated sidelobes. Fig. 4 is a plot of the computed phase error for a pulse-compression loop in which the expanded pulse is spectrally inverted and compressed in the same filter used for expansion. The associated recompressed pulse shown in Fig.

[3] Details of this modification are described in [2].

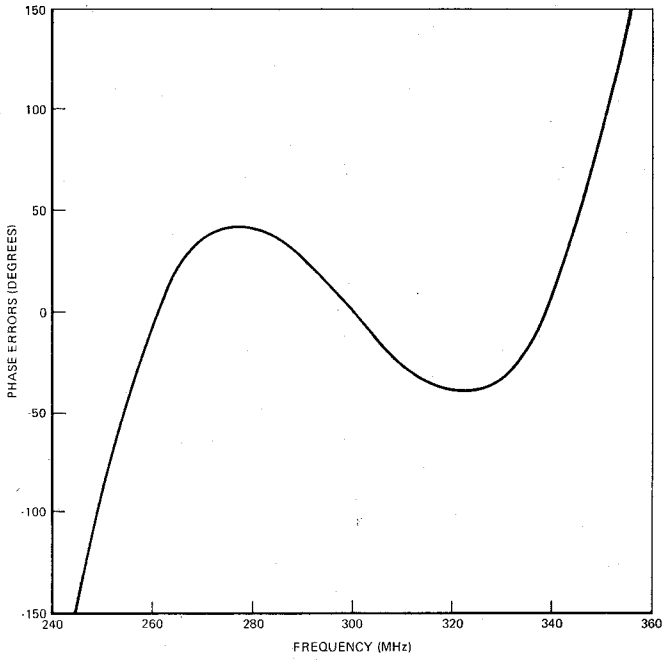

Fig. 4. Phase error caused by neglecting electric load interactions and acoustic velocity reduction in electrode regions in a 1000:1 filter used for both pulse expansion and compression.

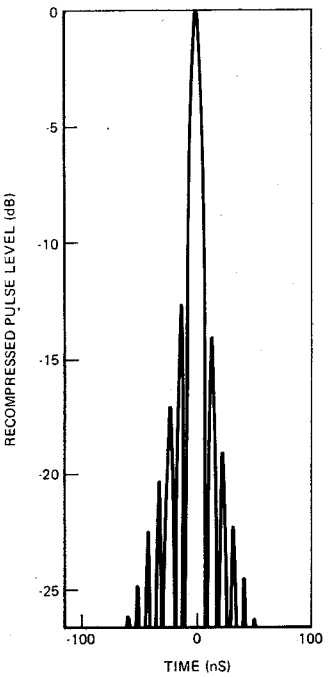

Fig. 6. Compressed pulse from a 1000:1 filter designed to account for electric-load interactions and acoustic velocity reduction in electrode regions.

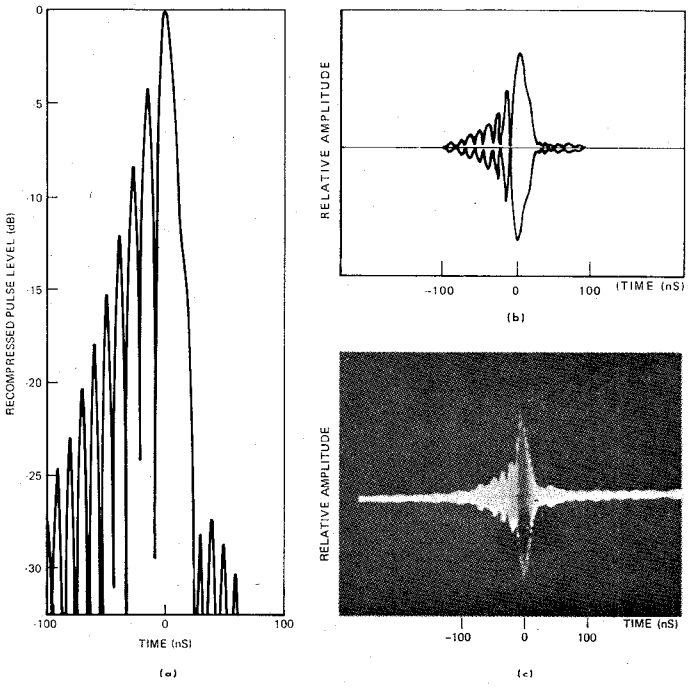

Fig. 5. Compressed pulse from a 1000:1 filter without correction for electric-load interactions and acoustic velocity reduction in electrode regions. (a) Calculated. (b) Calculated amplitude. (c) Observed amplitude.

5(a) and (b) is severely distorted from the desired sin x/x shape, with the largest leading sidelobe being only 4 dB below the main recompressed pulse. This result is essentially confirmed by the experimental data of Fig. 5(c), although the largest leading sidelobe is somewhat lower (−8 dB) than predicted.

When the transducer design is modified to account for coupling to the load and the electrode-region velocity reduction, the phase errors are reduced to less than 4° in the operating band of 250–350 MHz. The recompressed pulse (Fig. 6) very nearly conforms to a sin x/x shape. The 1-dB difference between the levels of the largest leading and trailing sidelobes is a consequence of additional load-interaction effects which are discussed in [2], but were not accounted for in the present design.[4] The acoustic-wave impedance discontinuities caused by the metal electrodes as well as acoustic-propagation loss have been neglected in the calculations described above, inasmuch as the purpose was to verify the value of the lossless discontinuity-free circuit-model analysis for transducer design. The circuit model is presently being used to investigate the combined effects of the impedance discontinuities, propagation loss, and matching circuits in order to further optimize transducer design. Insertion-loss data calculated with and without the impedance–discontinuity effect, but without considering acoustic propagation loss, are presented in [2, fig. 10].

V. 1000:1 Dispersive-Filter Performance

The performance of a large compression-ratio broad bandwidth dispersive filter designed for 100-MHz bandwidth at a center frequency of 300 MHz is discussed in this section. To obtain broad-band operation with low CW insertion loss, strong-coupling *YZ* lithium niobate was used. For the required bandwidth, insertion losses of less than 40 dB cannot be realized with a weak-coupling substrate such as quartz. The use of lithium niobate led to the unveiling of several interesting complications associated with the strong piezoelec-

[4] See [2, p. 463] for the discussion of the "radiation admittance" term which causes this effect.

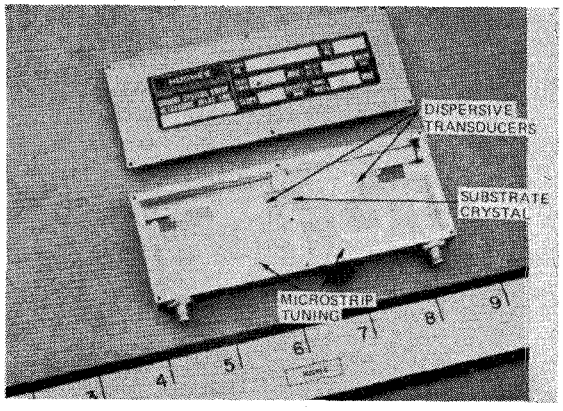

Fig. 7. Prototype 1000:1 dispersive filter with microstrip tuning circuits.

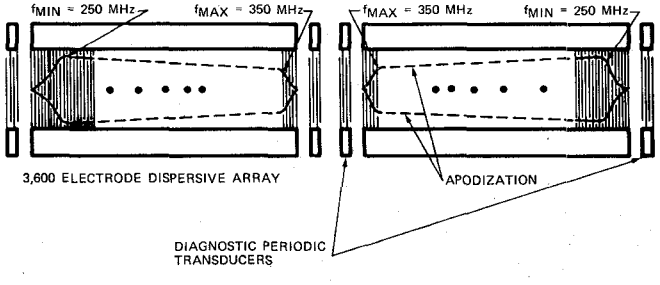

Fig. 8. 1000:1 dispersive-filter transducer geometry.

tric coupling. With appropriate compensations, however, the excellent observed performance demonstrates that strong-coupling materials are extremely valuable for complex pulse-compression filter applications. Moreover, the study of strong coupling effects has given valuable insights into similar effects that can cause problems in all extremely long dispersive filters, even when weak-coupling materials are used.

The prototype 1000:1 dispersive filter, shown in Fig. 7, includes the delay crystal with interdigital transducer arrays and the microstrip impedance matching transformers. The tapping electrodes in the input and output arrays are located on the acoustic substrate to yield a "down-chirp" linear FM waveform.

The transducer structures are fabricated from 750-Å aluminum, deposited using the "lift-off" or expendable-mask lithography technique [7]. This technique has proved most valuable in achieving uniform 2.5-μm widths for the required 7200 electrodes which are spaced over a pattern area of more than 2 in. The transducer geometry used in the 1000:1 design is shown schematically in Fig. 8. The choice of a down-chirp configuration is essential for the following reason. The metal electrodes on the surface of a strongly piezoelectric substrate cause wave-impedance discontinuities, resulting in undesirable surface-wave reflections [2], [8]. These reflections are of critical importance in the 1000:1 filter design since their magnitude is comparable to that for a periodic array of nearly 140 electrodes [5]. In linear FM transducers, these reflections introduce high directivity, enhancing the coupling of acoustic waves directed toward the high-frequency end and suppressing those directed toward the low-frequency end. The down-chirp configuration is therefore most desirable for low filter insertion loss.

Theoretical design considerations show that favorable source and load impedances for efficient operation of the transducers are considerably less than 50 Ω. The microstrip circuits provide an impedance reduction of approximately 17:1, thereby improving the efficiency of the dispersive filter. These circuits are composed of a quarter wavelength transmission line with a shorted stub, and are similar to those described in [15].

The measured CW insertion-loss spectrum of a typical tuned 1000:1 dispersive filter, shown in Fig. 9, exhibits a rectangular passband which conforms closely to the ideal shape for an unweighted expansion (transmitter) filter. The realization of insertion loss as low as 30 dB is very encouraging for a filter of such complexity, although the measured amplitude ripple of approximately ± 0.8 dB is slightly larger than predicted by the lossless transducer circuit model [2]. Triple-transit echoes, spurious signals, and direct electromagnetic feedthrough are typically suppressed by more than 50 dB. The departure of the measured phase response from an ideal quadratic phase function is also shown in Fig. 9. The dispersive filters were thermally insulated in order to prevent drifts during the 15 min required to complete the phase and amplitude measurement on a computer-controlled network analyzer.

Fig. 10 shows the impulse response, or expanded pulse, of the 1000:1 dispersive filter and the recompressed pulse envelope using the same filter to both expand and compress. Spectral inversion was employed prior to compression in order to transform the down-chirp linear FM into its matched "up-chirp" waveform. The nearly rectangular impulse response is consistent with the flat insertion-loss spectrum shown in Fig. 9. The sin x/x form of the recompressed pulse envelope is evidence that the amplitude and phase performance of the 1000:1 dispersive filter is nearly ideal. Some departure from a perfect sin x/x shape is, however, apparent in the more distant time sidelobes. The measured null width of 20 ns, Fig. 11(a), is in accord with the 100-MHz bandwidth.

The deviation of the recompressed waveform from a perfect sin x/x shape indicates that high time sidelobe suppression may be difficult to achieve. This conjecture is supported by the comparison of recompressed pulses for both unweighted and Hamming-weighted cases. The same dispersive filters were used for both measurements with the Hamming weighting implemented by means of a coaxial transmission-line transversal filter. Fig. 11(b) shows that Hamming weighting increases the null width of the recompressed pulse from 20 ns (unweighted) to 38 ns, and the time sidelobe suppression, from 13 dB (unweighted) to 27 dB. Theoretically, for a 1000:1 linear FM design, the use of Hamming spectral weighting is capable of 42-dB time sidelobe suppression with null width broadening by a factor of 2 [1], [9]. This discrepancy results from the amplitude and phase errors in the dispersive-filter response. Since the phase and amplitude variations (which are discussed in more detail below) are largely random, it does not seem likely that extending the design-compression ratio by increasing bandwidth or time dispersion will lead to further reduction in the achievable sidelobe suppression. While designs having compression ratios of more than 1000:1 are realizable, some question remains as to whether time sidelobe suppression in excess of about 30 dB can be achieved without the use of external equalization to compensate for the small variations in each filter response.

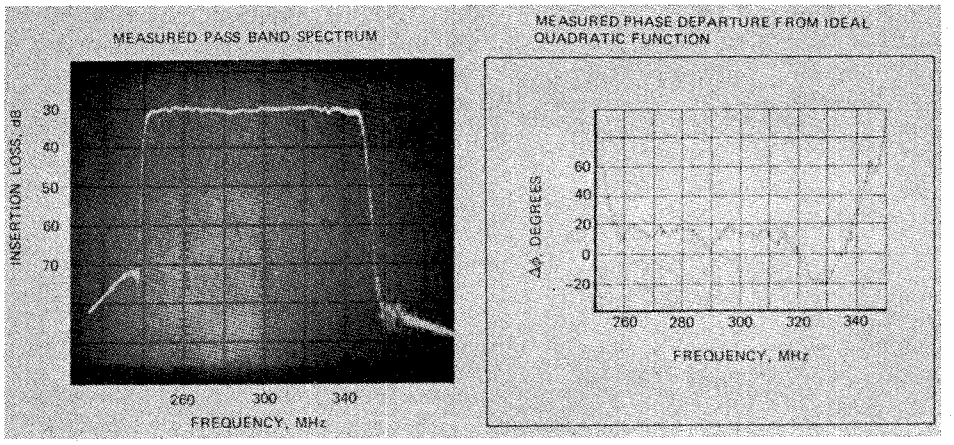

Fig. 9. Measured insertion-loss spectrum and phase deviation from a quadratic for 1000:1 linear FM dispersive filter.

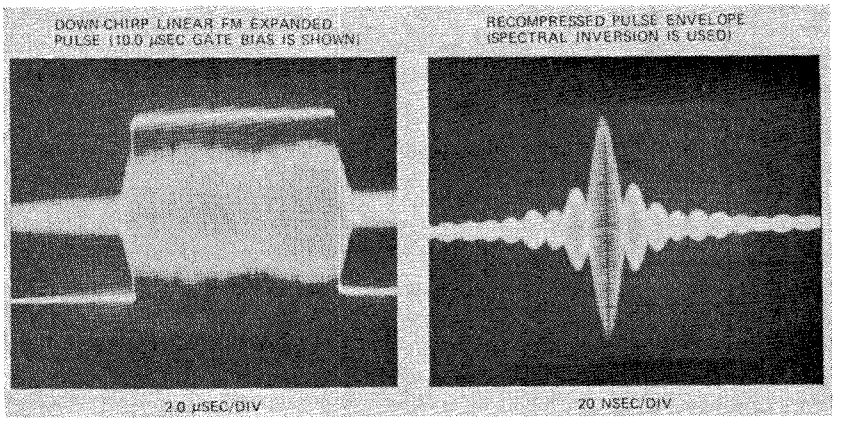

Fig. 10. Expanded and compressed pulse envelopes for unweighted 1000:1 linear FM dispersive filter.

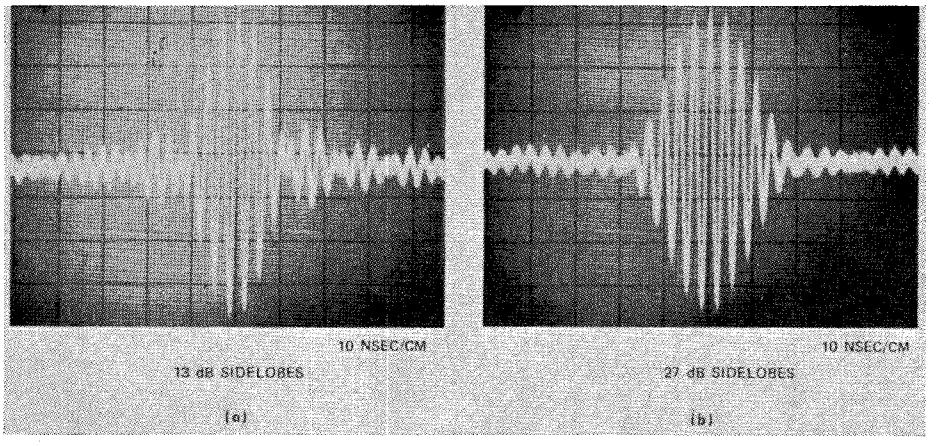

Fig. 11. Recompressed pulse waveforms. (a) With no spectral weighting. (b) With Hamming weighting.

A prototype compressive receiver which utilizes three 1000:1 linear FM dispersive filters has been assembled and tested. Two of these filters generate the sweeping local oscillator signal while the third is utilized to compress the IF mixer-output waveform (see Fig. 1). The operation of the microscan receiver was discussed in Section II. The necessity of maintaining high signal-to-noise ratios requires that all filters have low insertion loss. Specifically, the signal from the sweeping local oscillator into the mixer should be at least 10 dB above the maximum received signal to avoid degradation of the receiver performance.

Typical measured results are shown in Fig. 12(a) and (b). Fig. 12(a) shows the detected output of the compression filter for two equal-amplitude CW signals separated by 1 MHz. Fig. 12(b) shows the same situation with 400-kHz separation between signals. During these tests equal amplitude signals of −95 dBm were resolved down to a separation of 200 kHz. These encouraging results were obtained in spite of using dispersive filters which had small differences in chirp slope. The use of adjustable temperature-controlled ovens to achieve matching chirp slopes in the dispersive filters is expected to improve the resolution to 100 kHz.

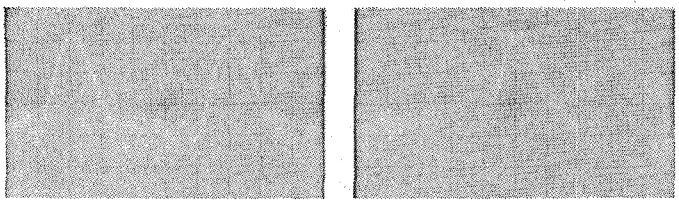

Fig. 12. Compressive receiver output pulses for CW signals separated by (a) 1 MHz. Time scale: 20 ns/div. Receiver units are −95 dBm. (b) 400 kHz. Time scale: 20 ns/div.

The foregoing discussion demonstrates that high-performance 1000:1 dispersive filters with low insertion loss can be realized. We now focus on the finer details of the filter behavior, with particular emphasis placed on the explanation of the losses and the factors which lead to errors and variations in the filter response.

Electrical impedance data have been used to estimate the conduction losses in an untuned dispersive transducer in the following manner. Within the range of 250–350 MHz, the total series resistance measured 1.8 Ω. Since circuit-model predictions indicate an acoustic radiation resistance of 0.62 Ω, the remaining resistance of approximately 1.2 Ω therefore corresponds to nonacoustic losses within the transducer. We can calculate the total loss for an untuned dispersive transducer. The transducer efficiency in terms of the generator impedance, R_G, the radiation resistance R_a, the conduction loss R_c, and the array capacitance C_T, is given by

$$E_T \simeq \frac{4R_G R_a}{(R_G + R_a + R_c)^2 + (1/\omega C_T)^2} . \qquad (5\text{-}1)$$

For $R_G = 50\ \Omega$, $R_c = 1.2\ \Omega$, $R_a = 0.6\ \Omega$, and $C_T = 160$ pF, the transducer loss is 14 dB. Of this, roughly 9 dB corresponds to electrical mismatch loss, and the remainder to conduction losses within the transducer. A 3-dB loss, which is commonly included to account for the bidirectional loss in conventional interdigital transducers, has not been included here because of the highly directional nature of the long transducers.

The microstrip networks are designed to reduce R_G to approximately 3 Ω, thereby improving the impedance match of the transducers. As a result, the tuning circuits provide a reduction in the filter insertion loss by approximately 15 dB. The realization of this large improvement required careful attention to the minimization of conduction losses in the microstrip circuits, since a circuit resistance of only a few ohms could easily negate any advantage gained by tuning.

The typical insertion loss for a tuned 1000:1 dispersive filter ranges between 30 and 35 dB. With transducer mismatch and conduction losses accounting for typically 13 dB, the remaining loss arises principally from the propagation loss of the acoustic wave within the electroded regions. Since long dispersive gratings are nearly periodic, they produce an almost perfect acoustic reflection (i.e., the reflection loss is very small). The triple-transit suppression in the 1000:1 dispersive filter is therefore approximately equal to twice the propagation loss between the points of reflection. Thus the propagation loss in the 1000:1 filter can be measured across the passband by simply observing the frequency-dependent time-delay characteristics of narrow-band tone pulses and measuring triple-transit echo suppression. The measured triple-transit suppression data, shown in Fig. 13, indicate that the propagation

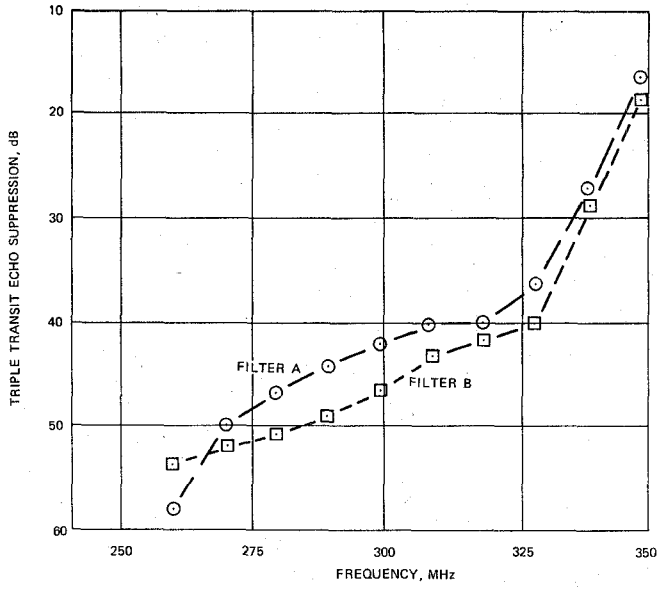

Fig. 13. Triple-transit echo suppression versus frequency measured in two different 1000:1 linear FM dispersive filters.

loss varies by about 5 dB over the passband. The relatively high measured midband propagation loss of 22–25 dB may indicate appreciable scattering of the surface wave into bulk waves within the arrays. The propagation loss is seen to decrease sharply at the upper edge of the passband where the distance of propagation within the electroded regions becomes small. Combining the propagation loss from Fig. 13 with the 13-dB total-tuned transducer loss, gives reasonably good agreement with the measured insertion loss. The corresponding loss for an untuned dispersive filter, in which the transducer loss is approximately 28 dB, also agrees well with measured values of typically 50 dB. The overall measured loss, as well as the details of the passband shape, have been found to vary by several decibels as a consequence of differences in the propagation loss within the electroded regions. The frequency dependence of the propagation loss appears to be intimately related to the nature of the metal electrodes. Anomalies in the passband shape, such as small peaks and valleys and the "non-Fresnel" shaped ripple may, therefore, be eliminated by improved fabrication uniformity.

Since the filter-loss characterization presented above does not shed much light on the nature of the filter-phase response, it yields little information about the pulse-compression performance of the 1000:1 dispersive filters. The factors which determine the filter-phase characteristics are the phase shifts associated with the transducer capacitance and matching circuits and the frequency dependence of the acoustic phase delay. The circuit effect is far smaller than the acoustic phase delay which contributes 2π for each acoustic wavelength in the delay path. For this reason, variations in the acoustic delay properties are the principal cause of the phase deviations observed in 1000:1 filters.

It is important to distinguish between "errors" and "variation" in the phase response. Errors are departures from quadratic frequency dependence of the phase, while variations refer to differences in the constants used to describe the quadratic phase functions of different filters. In general, small phase errors produce time sidelobes in the recompressed pulse whose size and position depend on the nature of the error [1]. The presence of these phase errors defeats the effectiveness of con-

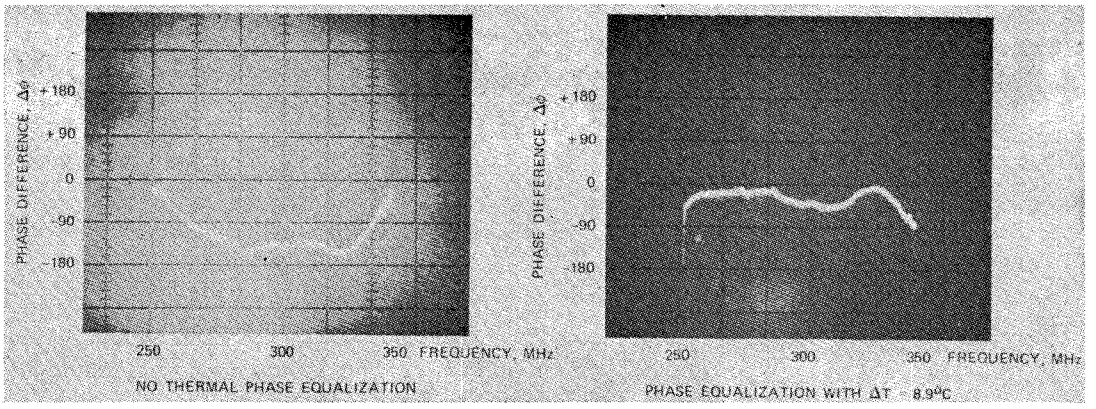

Fig. 14. Phase difference versus frequency between two 1000:1 linear FM dispersive filters before and after thermal chirp-slope equalization ($\Delta T = 8.9°C$).

ventional spectral weighting techniques for suppressing the 13-dB time sidelobes which are characteristic of a pair of perfect (error-free) matched linear FM filters.

Since accurate phase behavior is of primary importance in large compression-ratio dispersive filters, factors which lead to errors merit special attention.

Provided electrode positions are corrected to account for the constant width electrodes and other strong coupling effects discussed in Section IV, accurate phase response depends on transducer fabrication. Improper photoresist exposure, for example, may cause the actual electrode width to be in error by an amount ΔW. This causes the acoustic phase from the region of excitation to the high-frequency end of the array to change by

$$\Delta\phi(f) = 2\pi f\left\{\left[\frac{\Delta\tau}{\Delta f}\right][f - f'] + \left[\frac{\Delta W}{v_0}\right]\left[\frac{\delta v}{v_0}\right]\eta(f')\right\} \quad (5\text{-}2)$$

where

$$f' \simeq f\left\{1 + 2f\left[\frac{\Delta W}{v_0}\right]\left[\frac{\delta v}{v_0}\right]\right\}$$

and v_0 is the unmetallized surface-wave velocity, δv is the change in velocity resulting from shorting, and $\eta(f)$ is the number of electrodes between the point of excitation and the high-frequency end of the array. In the constant electrode-width arrays, the corrected electrode positions do not differ appreciably from the linear FM law; therefore,

$$\eta(f) \simeq 2\Delta\tau\left\{f_0 + \frac{[f_{\min}{}^2 - f^2]}{2\Delta f}\right\} \quad (5\text{-}3)$$

where $f_{\min}$ is the minimum frequency in the filter band and $\Delta\tau$ is twice the time dispersion for a single array. Since the dispersive filters are operated using spectral inversion to invert the passband about the center frequency f_0, the phase error is expressed with reference to the midband frequency. Of particular interest are the phase error terms in $(f-f_0)^2$ and $(f-f_0)^3$, which correspond to the changes in chirp slope and delay linearity, respectively. These terms are given by

$$\Delta\phi_2 \simeq 2\pi[f - f_0]^2\left[\frac{\Delta W}{W}\right]\left[\frac{\delta v}{v_0}\right]\left[\frac{9f_0}{4f_{\max}}\right]\left[\frac{\Delta\tau}{\Delta f}\right] \quad (5\text{-}4)$$

and

$$\Delta\phi_3 \simeq 2\pi[f - f_0]^3\left[\frac{\Delta W}{W}\right]\left[\frac{\delta v}{v_0}\right]\left[\frac{\Delta\tau}{\Delta f}\right]\left[\frac{3}{4f_{\max}}\right] \quad (5\text{-}5)$$

where $f_{\max}$ is the highest frequency in the filter band. The design electrode width W equals a quarter wavelength at $f_{\max}$. Thus the error in the phase response is proportional to both the fabrication tolerance $\Delta W/W$ and to $\delta v/v_0$.

Measurements of the phase response of the 1000:1 dispersive filters indicate that it can generally be fitted to within 20° of a quadratic curve centered at f_0. The constants defining the "best-fit" quadratics for different filters, however, vary over a range of almost 0.5 percent. Therefore, when two filters are operated as a matched pair they often exhibit a phase mismatch of several hundred degrees over the 100-MHz band.

From (5-4), the predicted chirp-slope error is related to $\Delta W/W$ by

$$\frac{\Delta \text{ chirp slope}}{\text{chirp slope}} = \frac{9}{2}\frac{f_0}{f_{\max}}\left[\frac{\delta v}{v_0}\right]\left[\frac{\Delta W}{W}\right]. \quad (5\text{-}6)$$

With $\delta v/v_0 \simeq 2.2\times10^{-2}$ for YZ $LiNbO_3$ [10], the observed chirp-slope variations of 0.5 percent correspond to $\Delta W/W \simeq 6$ percent. This is reasonable for the large number of filters tested with the substantial evolution of the fabrication processes. In the most recent filters, fabricated in pairs using identical photoresist exposures, the chirp-slope variations were found to correspond to electrode-width variations of less than 1.0 percent. This demonstrates that careful controls on fabrication can substantially overcome the phase mismatch problem.

Unless the phase discrepancies are corrected, the recompressed waveform may bear little resemblance to the desired $\sin x/x$ shape. Small differences in chirp slope $\Delta\tau/\Delta f$ can be corrected relatively easily by using broad-band electromagnetic dispersive networks, for example, which have quite modest compression ratios [9], [11]. An alternate approach to matching the phase responses utilizes the temperature dependence of the acoustic velocity. With the filters in separate ovens, the temperatures are adjusted until the quadratic phase difference is cancelled. Fig. 14 shows the measured phase difference as a function of frequency for two dispersive filters before and after temperature compensation. The temperature difference,

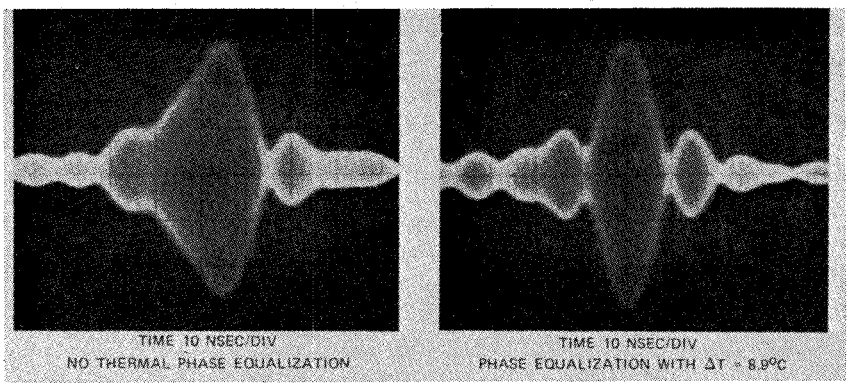

Fig. 15. Compressed pulse envelope for a pair of 1000:1 linear dispersive filters before and after thermal chirp-slope equalization ($\Delta T = 8.9°C$).

ΔT, to offset the chirp-slope difference is

$$\Delta T = -\frac{1}{2K}\left\{\frac{\Delta(\text{chirp slope})}{(\text{chirp slope})}\right\} \tag{5-7}$$

where K is the temperature coefficient of delay for the substrate material. For YZ $LiNbO_3$ with $K = -85 \times 10^{-6}/°C$, [12], chirp-slope variations of as much as 0.5 percent can be equalized with temperature differences of less than 30°C. Fig. 15 shows the improvement in the shape of the recompressed pulse of the two filters in Fig. 14 using temperature-controlled ovens.

Examination of the cubic-phase error term in (5-5) shows that, although its magnitude is smaller than the quadratic term by almost a factor of 20, it may cause serious problems when the fabrication errors are large.

In addition to the smooth phase variations described above, small random departures (errors) of the phase data from a quadratic-frequency dependence have been observed. Because these errors are not reproduced in different filters fabricated from the same mask, it is unlikely that they result from errors in the design or fabrication of the photomask. It is more plausible that the errors are caused by nonuniformities in the metal electrode structure. The dependence of phase error on electrode width, derived from (5-2) and (5-3), indicates that only a few percent change in W can produce an error of many degrees. In view of the magnitude of the measured phase errors of $\simeq 20°$, and the estimated fabrication tolerances, random variations in W offer a plausible explanation for these errors. When the variation in W is not uniform, the exact characterization of $\Delta\phi$ depends on the detailed nature of the variation and is not attempted here. The mathematical analysis of the consequences of a 20° nonperiodic phase error over the filter bandwidth has not been performed. However, experimental implementation of Hamming spectral weighting produced sidelobe suppression varying from 21 to 27 dB for different dispersive filters rather than the theoretical value of 42 dB.

In addition to reducing these errors by improved fabrication accuracy, a second approach may be to utilize a weaker coupling substrate to decrease $\delta v/v_0$. In so doing, the filter insertion loss is generally increased. Thus, for each specific application there is a tradeoff between the advantages of improved signal-to-noise ratio due to low loss and the disadvantages of poor time sidelobe suppression due to phase errors.

VI. Conclusions

Acoustic surface-wave technology has for several years promised to revolutionize the design of complex filters at IF and high IF frequencies. The realization of a 100-MHz bandwidth, low insertion-loss dispersive filter indicates that these expectations are well on their way to being realized. This is not to imply that all the problems have been solved, but rather that continued effort in characterizing acoustic losses and improving fabrication controls will be rewarded.

We have shown that present phenomenological computer models are sufficiently versatile to cope with the second-order effects encountered with strong-coupling piezoelectrics. However, considerable work remains to be done in treating conduction and propagation losses in complex acoustic surface-wave filters.

The performance of the 1000:1 dispersive filter was shown to be highly encouraging with the remaining problems stemming primarily from fabrication variations. These difficulties might be substantially reduced with improvement of photolithography procedures, such as the use of flexible glass photomasks [13]. The use of a weak-coupling substrate can effect a reduction in errors in the filter response; however, this approach may increase the filter insertion loss.

The development of accurate and reproducible dispersive filters having compression ratios on the order of 1000 is the first step toward meeting future dispersive-filter requirements of TB's > 10 000. The passive chirp-sweep generator in the compressive receiver demonstrates that identical 1000:1 filters may be used to provide an increased compression ratio. This general technique of using N linear FM dispersive filters to enhance the compression ratio by a factor of N^2, has been proven at low frequencies using 100:1 filters with $N = 10$ [14]. From the performance of the two 1000:1 filters in the compressive receiver (which were not phase compensated in ovens), the prospects seem excellent for combining several of the 1000:1 components to achieve TB = 10 000 or more.

Finally, it should be mentioned that a novel transducer geometry employing eighth wave or "double" electrodes has recently been reported in conjunction with the suppression of electrode reflections. It was demonstrated that transducers utilizing this geometry exhibit strong responses at their third harmonic. This double-electrode geometry may be utilized to great advantage in the design of highly dispersive filters since the suppression of electrode reflections helps to improve the triple-transit echo rejection. Even more significant is the fact

that harmonic operation permits the upper frequency range of fabrication to be extended for most dispersive-filter designs [4].

In view of the wide utility of large TB dispersive filters having high compression ratios and the degree of success in present development efforts, the outlook is extremely bright for continued progress in the field of acoustic surface-wave dispersive filters.

Acknowledgment

The authors wish to thank R. L. Lanphar for his assistance in the computational work and W. K. Masenten for his critical reading of the manuscript.

References

[1] J. R. Klauder, A. C. Price, S. Darlington, and W. J. Albersheim, "The theory and design of chirp radars," *Bell Syst. Tech. J.*, vol. 34, pp. 745–808, July 1960.
[2] W. R. Smith, H. M. Gerard, and W. R. Jones, "Analysis and design of dispersive interdigital surface-wave transducers," *IEEE Trans. Microwave Theory Tech.*, vol. MTT-20, pp. 458–471, July 1972.
[3] R. H. Tancrell and M. G. Holland, "Acoustic surface wave filters," *Proc. IEEE*, vol. 59, pp. 393–409, Mar. 1971.
[4] T. W. Bristol, W. R. Jones, G. W. Judd, and W. R. Smith, "Further applications of double electrodes in acoustic surface wave device design," presented at the 1972 IEEE G-MTT Int. Microwave Symp.
[5] E. K. Sittig and G. A. Coquin, "Filters and dispersive delay lines using repetitively mismatched ultrasonic transmission lines," *IEEE Trans. Sonics Ultrason.*, vol. SU-15, pp. 111–119, Apr. 1968.
[6] W. R. Smith, *et al.*, "Analysis of interdigital surface wave transducers by use of an equivalent circuit model," *IEEE Trans. Microwave Theory Tech.*, vol. MTT-17, pp. 856–864, Nov. 1969.
[7] M. K. Stelter, "Chrome etching and relief deposition," *J. Photochem. Etching*, vol. 1, pp. 4–6, Dec. 1966.
[8] W. S. Jones, C. S. Hartman, and T. D. Sturdivant, "Second order effects in surface wave devices," *IEEE Trans. Sonics Ultrason.*, SU-19, pp. 368–377, July 1972.
[9] C. E. Cook and M. Bernfeld, *Radar Signals*. New York: Academic Press, Inc., 1967.
[10] J. J. Campbell and W. R. Jones, "A method for estimating optimal crystal cuts and propagation directions for excitation of piezoelectric surface waves," *IEEE Trans. Sonics Ultrason.*, vol. SU-15, pp. 209–217, Oct. 1968.
[11] T. R. O'Meara, "The synthesis of 'band pass' all-pass time delay networks with graphical approximation techniques," Hughes Res. Lab., Malibu, Calif., Rep. 114, 1962.
[12] J. D. Maines, E. G. S. Paige, A. F. Saunders, and A. S. Young, "Simple technique for the accurate determination of delay-time variations in acoustic-surface-wave structures," *Electron. Lett.*, vol. 5, pp. 678–680, Dec. 1969.
[13] H. I. Smith, F. J. Bachner, and N. Efremow, "A high-yield photolithographic technique for surface wave devices," *J. Electrochem. Soc.*, vol. 118, pp. 821–825, May 1971.
[14] R. D. Haggarty, L. A. Hart, and G. C. O'Leary, "A 10,000:1 pulse compression filter using a tapped delay line linear filter synthesis technique," in *EASCON Rec.*, pp. 306–314, 1968.
[15] T. M. Reeder and W. R. Sperry, "Broad-band coupling to high-Q resonant loads," *IEEE Trans. Microwave Theory Tech.*, vol. MTT-20, pp. 453–458, July 1972.
[16] H. Urkowitz, "Ambiguity and resolution," in *Modern Radar*, R. S. Berkowitz, Ed. New York: Wiley, 1965, pp. 197–203.

The IMCON Pulse Compression Filter and its Applications

TOM A. MARTIN

Invited Paper

***Abstract*—The IMCON is a reflection-mode dispersive delay line capable of high performance in large time–bandwidth product pulse compression systems. As developed in this paper, the unique characteristics of the IMCON are obtained by reflection from a double grating array that is applied to the surface of a strip. Current models of the device have center frequencies in the 4–30-MHz range with bandwidth up to 15 MHz, dispersion to 320 μs, time sidelobes on the order of −40 dB (with equalization), and other spurious signals at least 70 dB below the compressed output.**

The characteristics of IMCON operation are developed from a consideration of the device's transfer function. In particular, the IMCON's high linearity and low sensitivity to fabrication and propagation problems are shown to be due to a unique error rejection effect. By comparison, the error rejection characteristics of single grating and dispersive transducer devices are found to be inferior to the IMCON. Data derived from operating pulse compression systems are utilized to demonstrate the low time sidelobe and high time–bandwidth capability of the IMCON.

Manuscript received September 18, 1972; revised October 26, 1972.
The author is with Andersen Laboratories, Inc., Bloomfield, Conn. 06002.

I. Introduction

THE IMCON is a reflection-mode dispersive delay line capable of high performance in large time–bandwidth pulse compression systems [1]. It has evolved from a synthesis of three earlier dispersive delay-line technologies: the dispersive strip delay line, the perpendicular diffraction delay line, and the reflection grating device of Sittig and Coquin.

The dispersive strip delay line, described by Meeker [2], makes use of the naturally dispersive characteristics of the first symmetric Lamb mode in a thin strip of metal. Although